

S.V. BEKH,¹ A.P. KOBUSHKIN,^{2,1} E.A. STROKOVSKY^{3,4}¹National Technical University of Ukraine “Igor Sikorsky Kiev Polytechnic Institute”
(37, Prospect Peremogy, 03056 Kiev, Ukraine; e-mail: bekh@bitp.kiev.ua)²Bogolyubov Institute for Theoretical Physics, Nat. Acad. of Sci. of Ukraine
(14b, Metrolohichna Str., Kiev 03143, Ukraine; e-mail: kobushkin@bitp.kiev.ua)³Laboratory of High Energy Physics, Joint Institute for Nuclear Research
(141980, Dubna, Russia; e-mail: strok@jinr.ru)⁴Research Center for Nuclear Physics, Osaka University
(10-1 Mihogaoka, Ibaraki, Osaka, 567-0047, Japan)**Nucleon momentum distributions in ${}^3\text{He}$ and three-body interactions**PACS 21.45.-v, 21.45.Dc,
21.45.Ff, 24.10.Jv

We calculate the momentum distributions of neutrons and protons in ${}^3\text{He}$ in the framework of a model which includes 3N interactions together with 2N interactions. It is shown that the contribution of 3N interactions becomes essential in comparison with that coming from 2N interactions for the internal momentum in ${}^3\text{He}$ $k > 250$ MeV/c. We also compare the calculated momentum distribution of protons with the so-called empirical momentum distribution of protons extracted from the $A({}^3\text{He}, p)$ breakup cross-sections measured for protons emitted at zero degree. It is concluded that 3N interactions cannot completely explain the disagreement between the available data on the empirical momentum distribution of protons in ${}^3\text{He}$ and calculations based on 2N interactions, which is observed at the high momentum region of the momentum distribution, $k > 250$ MeV/c.

Keywords: nucleon momentum distributions, empirical momentum distribution, three-body interactions.

1. Introduction

Momentum distributions of nucleons in nuclei are directly connected with the spatial structure of the corresponding nuclear systems. In particular, these distributions at Fermi momenta above 200-300 MeV/c (this region is usually referred to as “a region of high relative nucleon momenta”) give important information about such interesting questions as a role of non-nucleon degrees of freedom in the nuclear structure, relativistic effects, and so on.

Starting from three nucleon systems, ${}^3\text{He}$ and ${}^3\text{H}$, the momentum distributions should also give information about the role of effective three-nucleon (3N)

interactions in nuclear structure. For example, a prominent role of 3N interactions was demonstrated in a systematic study of the elastic scattering of polarized protons from deuterons at energies from 100 to 200 MeV [1]. Besides that, the relativistic effects are also important in 3N systems, see, e.g., the results of recent relativistic calculations of the triton binding energy [2] with the so-called Kharkov potential, one-boson-exchange NN potential constructed with use of an unitary clothing transformation [3].

The goals of this paper are:

1. to find signals of manifestation of 3N interactions in the momentum distributions of neutrons and protons in ${}^3\text{He}$,

2. to compare theoretical results, coming from known models for 2N+3N interactions, with existing experimental data,
3. to indicate what region of relative nuclear momenta should be looked for manifestations of non-nucleonic degrees of freedom in the nuclear structure.

The paper is organized in the following way. We start, in Section 2, with a short overview of the operator form of a three nucleon bound state, which is a basic point for further calculations. In Section 3, the momentum distribution of neutrons in ${}^3\text{He}$ is calculated within a model, which takes into account 3N interactions together with the standard 2N interactions.

In Section 4, the momentum distribution of protons in ${}^3\text{He}$ is calculated in the framework of a similar model. The calculated proton momentum distribution is compared with existing experimental data in Section 5, namely: in Subsection 5.1, we discuss the definition and a procedure of extraction of the so-called “empirical momentum distribution” of protons in ${}^3\text{He}$ from the $A({}^3\text{He}, p)$ breakup cross-sections [4], when the proton-spectator was emitted at 0° ; in Subsection 5.2, the empirical momentum distribution is compared with the results of our calculations, as well as with calculations without explicit inclusion of 3N interactions. Conclusions are given in Section 6.

2. Operator form of three nucleon bound state

There are few known approaches to describe a three nucleon (3N) wave function: a partial wave decomposition (see, e.g., Ref. [5]), tensor representations [6–8], and an operator form [9]. In this paper we use the last one.

In 1942 E. Gerjuoy and J. Schwinger introduced an operator form for three- and four-nucleon states [9], which was a generalization of an operator form of the deuteron state elaborated earlier by W. Rarita and J. Schwinger [10]. In the case of a 3N nucleon state, this approach expresses the general spin structure of a 3N system in terms of nine operator forms acting on the special spin state, where nucleons 1 and 2 have the total spin $s = 0$ and nucleon 3 carries out the spin

of the 3N system:

$$|\nu\rangle = \frac{1}{\sqrt{2}}(|+ - \text{sign } \nu\rangle - |- + \text{sign } \nu\rangle). \quad (1)$$

In Eq. (1) ν is the magnetic quantum number of the 3N system and

$$|\text{sign } m_1 \text{ sign } m_2 \text{ sign } m_3\rangle$$

is a spin wave function of three nucleons with magnetic quantum numbers m_1 , m_2 , and m_3 .

The operator form does not employ the isospin formalism, and the nucleons are labelled as follows:

$$\begin{aligned} N_1 = N_2 = p \text{ and } N_3 = n & \quad \text{— for } {}^3\text{He}, \\ N_1 = N_2 = n \text{ and } N_3 = p & \quad \text{— for } {}^3\text{H}. \end{aligned}$$

The relations between approaches, which employ (or do not employ) the isospin formalism, as well as advantages of the latter ones, were discussed in Refs. [11, 12].

It was mentioned in Ref. [13], that the ninth spin structure of the operator form of a 3N system is redundant and we, following to Ref. [13], omit this component.

Finally, the 3N bound state wave function is given by

$$\Psi_\nu(\mathbf{p}, \mathbf{q}) = \sum_{i=1}^8 \phi_i(p, q, x) |i, \nu\rangle, \quad (2)$$

where $|i, \nu\rangle$ are the spin wave functions defined below (see, Eqs. (4)), \mathbf{p} and \mathbf{q} are the Jacobi momenta

$$\begin{aligned} \mathbf{p}_1 = \frac{1}{3}\mathbf{P} - \frac{1}{2}\mathbf{q} + \mathbf{p}, \quad \mathbf{p}_2 = \frac{1}{3}\mathbf{P} - \frac{1}{2}\mathbf{q} - \mathbf{p}, \\ \mathbf{p}_3 = \frac{1}{3}\mathbf{P} + \mathbf{q}. \end{aligned} \quad (3)$$

Here, \mathbf{p}_1 , \mathbf{p}_2 , and \mathbf{p}_3 are the momenta of the nucleons, and \mathbf{P} is the momentum of the nucleus; $x = \cos \kappa$ (κ is the angle between the vectors \mathbf{p} and \mathbf{q}), and $\phi_i(p, q, x)$ are scalar functions. The scalar functions $\phi_i(p, q, x)$ have been calculated in Ref. [13] for two modern potentials: the 2N potential AV18 [14] with the 3N potential Urbana-IX [15] (AV18+U9) and the 2N potential CD-Bonn [16] with the 3N potential Tucson-Melbourne [17] (CDBN+TM). The functions $\phi_i(p, q, x)$ are tabulated on a 3-dimensional grid (x, q, p) and can be downloaded from site [18].

The spin structures are given as follows:

$$\begin{aligned}
|1\nu\rangle &= |\nu\rangle, \quad |2\nu\rangle = \sqrt{\frac{1}{3}}(\boldsymbol{\sigma}(12) \cdot \boldsymbol{\sigma}(3)) |\nu\rangle, \\
|3\nu\rangle &= -i\sqrt{\frac{3}{2}}(\boldsymbol{\sigma}(3) \cdot (\hat{\mathbf{p}} \times \hat{\mathbf{q}})) |\nu\rangle, \\
|4\nu\rangle &= \sqrt{\frac{1}{2}} [i\boldsymbol{\sigma}(12) + (\boldsymbol{\sigma}(12) \times \boldsymbol{\sigma}(3))] \cdot (\hat{\mathbf{p}} \times \hat{\mathbf{q}}) \\
&\quad \times |\nu\rangle, \\
|5\nu\rangle &= [-i\boldsymbol{\sigma}(12) + \frac{1}{2}(\boldsymbol{\sigma}(12) \times \boldsymbol{\sigma}(3))] \cdot (\hat{\mathbf{p}} \times \hat{\mathbf{q}}) \\
&\quad \times |\nu\rangle, \\
|6\nu\rangle &= \sqrt{\frac{3}{2}} [(\boldsymbol{\sigma}(12) \cdot \hat{\mathbf{p}})(\boldsymbol{\sigma}(3) \cdot \hat{\mathbf{p}}) - \frac{1}{3}(\boldsymbol{\sigma}(12) \cdot \boldsymbol{\sigma}(3))] \\
&\quad \times |\nu\rangle, \\
|7\nu\rangle &= \sqrt{\frac{3}{2}} [(\boldsymbol{\sigma}(12) \cdot \hat{\mathbf{q}})(\boldsymbol{\sigma}(3) \cdot \hat{\mathbf{q}}) - \frac{1}{3}(\boldsymbol{\sigma}(12) \cdot \boldsymbol{\sigma}(3))] \\
&\quad \times |\nu\rangle, \\
|8\nu\rangle &= \frac{3}{2\sqrt{5}} [(\boldsymbol{\sigma}(12) \cdot \hat{\mathbf{q}})(\boldsymbol{\sigma}(3) \cdot \hat{\mathbf{p}}) \\
&\quad + (\boldsymbol{\sigma}(12) \cdot \hat{\mathbf{p}})(\boldsymbol{\sigma}(3) \cdot \hat{\mathbf{q}}) - \frac{2}{3}(\hat{\mathbf{p}} \cdot \hat{\mathbf{q}})(\boldsymbol{\sigma}(12) \cdot \boldsymbol{\sigma}(3))] |\nu\rangle,
\end{aligned} \tag{4}$$

where $\hat{\mathbf{q}} = \mathbf{q}/|\mathbf{q}|$, $\hat{\mathbf{p}} = \mathbf{p}/|\mathbf{p}|$, and

$$\boldsymbol{\sigma}(12) = \frac{1}{2}[\boldsymbol{\sigma}(1) - \boldsymbol{\sigma}(2)]; \tag{5}$$

$\boldsymbol{\sigma}(i)$ are the Pauli matrices of i -th nucleon.

The normalization of the wave function is given by

$$\begin{aligned}
&\int d^3q d^3p |\Psi_\nu(\mathbf{p}, \mathbf{q})|^2 \\
&= 8\pi^2 \int_{-1}^1 dx \int_0^\infty dq q^2 \int_0^\infty dp p^2 \\
&\times \left[\sum_{i=1}^8 \langle i\nu | i\nu \rangle \phi_i^2(p, q, x) \right. \\
&\quad \left. + 2 \sum_{i \neq j} \langle i\nu | j\nu \rangle \phi_i(p, q, x) \phi_j(p, q, x) \right] = 1.
\end{aligned} \tag{6}$$

Overlaps of the spin structures are given in Table 1.

Note that the contributions of $\phi_3(p, q, x)$, $\phi_4(p, q, x)$, and $\phi_5(p, q, x)$ to the normalization relation (6) are of order of $\sim 0.05\%$ and we ignore these components of the trinucleon wave function in Table 1, as well as in the subsequent calculations.

We have found that the results of numerical calculations, published in Refs. [13, 18], are represented on the 3-dimensional grid (p, q, x) which is not ‘‘dense’’ enough for needs of our calculations.

Table 1. Overlaps of the spin structures $\langle i\nu | j\nu \rangle$. Only nonvanishing overlaps are presented.

i	j	$\langle i\nu j\nu \rangle$	i	j	$\langle i\nu j\nu \rangle$
1	1	1	6	8	$\sqrt{\frac{6}{5}}x$
2	2	1	7	7	1
6	6	1	7	8	$\sqrt{\frac{6}{5}}x$
6	7	$\frac{1}{2}(3x^2 - 1)$	8	8	$\frac{9}{10}(1 + \frac{1}{3}x^2)$

Therefore we expanded the scalar functions $\phi_i(p, q, x)$ at fixed p and q in series in terms of the Legendre polynomials $P_\ell(x)$:

$$\begin{aligned}
\phi_1(p, q, x) &= C_{10}(p, q) + C_{12}(p, q)P_2(x), \\
\phi_2(p, q, x) &= C_{21}(p, q)P_1(x) + C_{23}(p, q)P_3(x), \\
\phi_3(p, q, x) &= C_{31}(p, q)P_1(x), \\
\phi_4(p, q, x) &= C_{40}(p, q) + C_{42}(p, q)P_2(x), \\
\phi_5(p, q, x) &= C_{50}(p, q) + C_{52}(p, q)P_2(x), \\
\phi_6(p, q, x) &= C_{61}(p, q)P_1(x), \\
\phi_7(p, q, x) &= C_{71}(p, q)P_1(x), \\
\phi_8(p, q, x) &= C_{80}(p, q) + C_{82}(p, q)P_2(x).
\end{aligned} \tag{7}$$

Terms with the Legendre polynomials of higher orders on ℓ were found to be negligibly small and will be omitted in the present numerical calculations. For example, in case of functions ϕ_3 , ϕ_6 , and ϕ_7 , the numerical coefficients for the next term, containing $P_3(x)$, were found approximately in $10^{-5} - 10^{-6}$ times less than $C_{31}(p, q)$, $C_{61}(p, q)$, and $C_{71}(p, q)$, respectively.

The coefficients $C_{m\ell}(p, q)$ of the series form 13 functions given on a 2-dimensional grid (p, q) .

3. Momentum distribution of neutrons in ${}^3\text{He}$

The momentum distribution of a neutron in ${}^3\text{He}$ is defined as follows (see [13]):

$$\begin{aligned}
n(K) &= \frac{1}{2} \sum_\nu \int d^3p d^3q \delta(\mathbf{q} - \mathbf{K}) |\Psi_\nu(\mathbf{p}, \mathbf{q})|^2 \\
&= \int d^3p \left| \Psi_{\frac{1}{2}}(\mathbf{p}, \mathbf{K}) \right|^2,
\end{aligned}$$

\mathbf{K} is the neutron momentum inside ${}^3\text{He}$. The factor $\frac{1}{2}$ comes from averaging over the nucleus magnetic

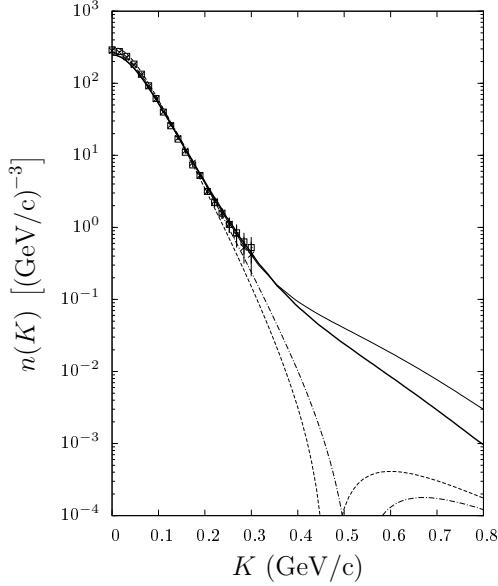


Fig. 1. Momentum distribution of neutrons in ${}^3\text{He}$ calculated with 2N+3N interactions, AV18+U9 (thin solid line) and CDBN+TM (thick solid line). The results obtained with 2N interactions only (dashed and dot-dashed lines, for the Paris [21] and CD-Bonn [16] potentials, respectively) are taken from Ref. [19]. The squares and crosses represent the results of variational calculations [20] obtained with the Urbana+U9 and Argonne+U9 interactions, respectively.

quantum numbers. Using the spin structures $\langle i\nu|j\nu\rangle$ from Table 1, we get

$$n(K) = 2\pi \int_0^\infty p^2 dp \int_{-1}^1 dx \rho_n(p, K, x), \quad (8)$$

where

$$\begin{aligned} \rho_n(p, K, x) = & \phi_1^2(p, K, x) + \phi_2^2(p, K, x) \\ & + \phi_6^2(p, K, x) + \phi_7^2(p, K, x) \\ & + \frac{9}{10} \left(1 + \frac{1}{3}x^2\right) \phi_8^2(p, K, x) \\ & + (-1 + 3x^2) \phi_6(p, K, x)\phi_7(p, K, x) \\ & + \sqrt{\frac{24}{5}}x [\phi_6(p, K, x) + \phi_7(p, K, x)] \phi_8(p, K, x). \end{aligned} \quad (9)$$

The resulting neutron momentum distribution, $n(K)$, for AV18+U9 and CDBN+TM together with the results of variational calculations from Ref. [20], are shown in Fig. 1. We compare this result with calculations from Ref. [19] obtained without 3N interactions. Good agreement between the results, obtained with and without 3N interactions, is obvious

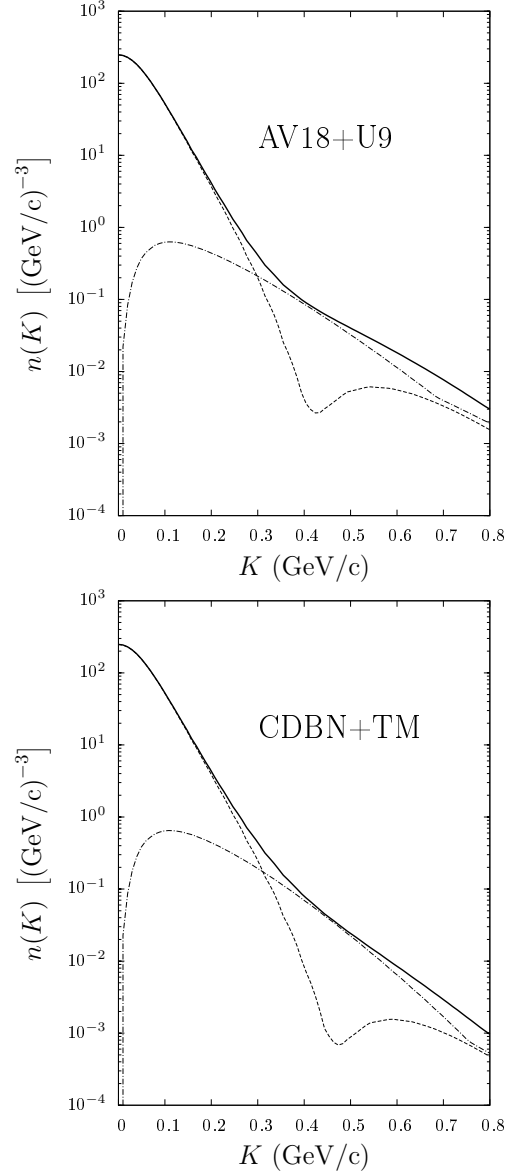


Fig. 2. Contributions of the main spin structures to the neutron momentum distribution in ${}^3\text{He}$. Dashed line: $(\phi_1)^2$; dot-dashed line: sum of contributions coming from $(\phi_{2,6,7,8})^2$ and interference terms $\phi_6\phi_7$, $\phi_6\phi_8$, $\phi_7\phi_8$; solid line: the result with all the terms taken into account.

for $K \lesssim 250$ MeV/c and demonstrates that 3N interactions do not manifest itself in this region. At higher K , the contribution of 3N interactions becomes significant and dominates from $K \sim 400$ MeV/c over the one from 2N interactions.

The contribution of the most important term, $(\phi_1)^2$, and the sum of other terms in Eq. (9) to the total momentum distribution are displayed in Fig. 2. It is worthwhile to note that contribution of the $(\phi_1)^2$ term has a dip in the same region (near $K \sim 450$ MeV/c), where the similar dip appears in calculations without 3N interactions.

4. Momentum distribution of protons in ${}^3\text{He}$

The momentum distribution of protons in ${}^3\text{He}$ is given by

$$n_p(K) = \frac{1}{2} \sum_{\nu} \int d^3p d^3q [\delta(\mathbf{p}_1 - \mathbf{K}) + \delta(\mathbf{p}_2 - \mathbf{K})] \times |\Psi_{\nu}(\mathbf{p}, \mathbf{q})|^2, \quad (10)$$

where \mathbf{K} is the proton momentum in ${}^3\text{He}$ and the factor $\frac{1}{2}$ comes from averaging over the nucleus magnetic quantum numbers. Due to identity of the protons, this expression is reduced to

$$\begin{aligned} n_p(K) &= \sum_{\nu} \int d^3p d^3q \delta(\mathbf{p}_1 - \mathbf{K}) |\Psi_{\nu}(\mathbf{p}, \mathbf{q})|^2 \\ &\equiv \sum_{\nu} \int d^3p d^3q \delta(\mathbf{p} - \frac{1}{2}\mathbf{q} - \mathbf{K}) |\Psi_{\nu}(\mathbf{p}, \mathbf{q})|^2 \\ &= 2 \int d^3p d^3q \delta(\mathbf{p} - \frac{1}{2}\mathbf{q} - \mathbf{K}) \rho_p(p, q, x) \\ &= 32\pi \int_0^{\infty} dp p^2 \int_{-1}^1 d \cos \theta_p \rho_p(p, q, x), \end{aligned} \quad (11)$$

where θ_p is angle between \mathbf{p} and \mathbf{K} , and

$$\begin{aligned} \rho_p(p, q, x) &= [C_{10}(p, q) + P_2(x)C_{12}(p, q)]^2 \\ &\quad + [P_1(x)C_{21}(p, q) + P_3(x)C_{23}(p, q)]^2 \\ &\quad + P_1^2(x) [C_{61}^2(p, q) + C_{71}^2(p, q)] \\ &\quad + \frac{9}{10} (1 + \frac{1}{3}x^2) [C_{80}(p, q) + P_2(x)C_{82}(p, q)]^2 \\ &\quad + (-1 + 3x^2) P_1^2(x) C_{61}(p, q) C_{71}(p, q) \\ &\quad + \sqrt{\frac{24}{5}} x P_1(x) [C_{61}(p, q) + C_{71}(p, q)] \\ &\quad \quad \times [C_{80}(p, q) + P_2(x)C_{82}(p, q)]. \end{aligned} \quad (12)$$

In the final line of Eq. (11), q and x are considered as functions of K , p , and θ_p .

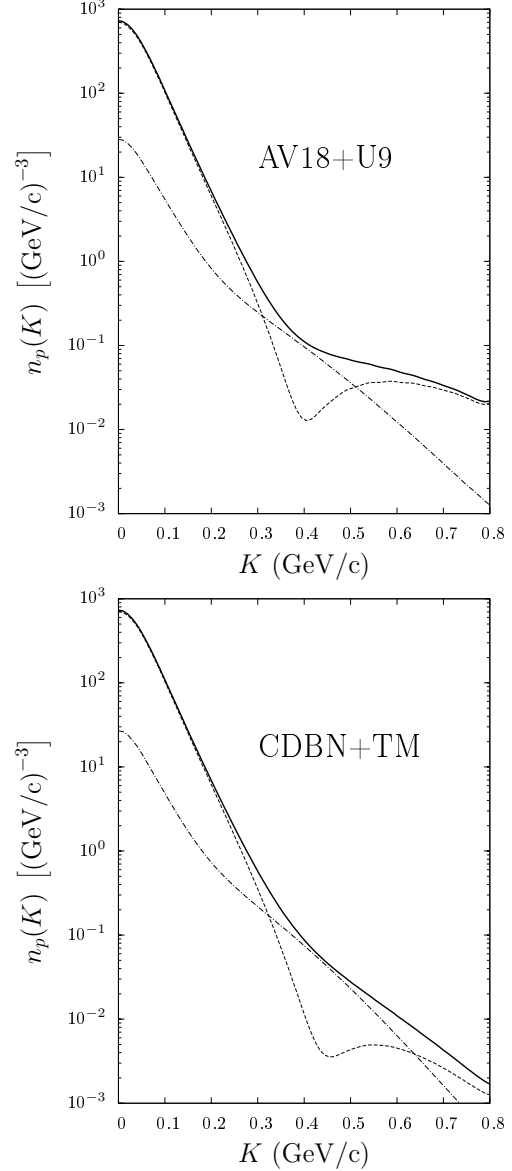


Fig. 3. Contributions of the main spin structures to the proton momentum distribution in ${}^3\text{He}$. The notations are the same as those in Fig. 2.

Using $\mathbf{K} = \mathbf{p} - \frac{1}{2}\mathbf{q}$, we get

$$\begin{aligned} q &= 2\sqrt{K^2 + p^2 - 2Kp \cos \theta_p}, \\ x &= \frac{p - K \cos \theta_p}{\sqrt{K^2 + p^2 - 2Kp \cos \theta_p}}. \end{aligned} \quad (13)$$

On the 2-dimensional grid, the integral over dp can be reduced to the sum $\sum_{i=1}^{n_p} w_i$, where w_i is an element

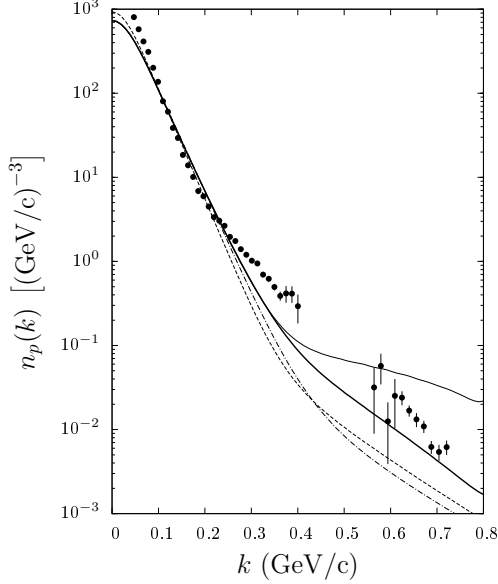


Fig. 4. Momentum distribution of protons in ${}^3\text{He}$ calculated with $2N+3N$ interactions. The notations of the curves are the same as those in Fig. 1. Circles represent the empirical momentum distribution extracted from the experimental data [4]. Here, k is the LFD variable, as defined in Section 5.

on the grid (p, q, x) . In turn, the integral over $d \cos \theta_p$ becomes

$$\int_{-1}^1 d \cos \theta_p P_{\ell_1}(x) P_{\ell}(x) C_{m\ell_1}(q, p_i) C_{m'\ell'}(q, p_i). \quad (14)$$

The variables x and q are defined by Eqs. (13), therefore q cannot be on the grid (p, q, x) . Nevertheless, the functions $C_{m\ell_1}(q, p_i)$ and $C_{m'\ell'}(q, p_i)$ at fixed p_i , K , and $\cos \theta_p$ can be obtained by a linear interpolation from their values given on the grid (q, p) .

The contribution of the spin structure 1 and sum of contributions coming from the spin structures 2, 6, 7, and 8 to the momentum distribution of protons in ${}^3\text{He}$ are displayed in Fig. 3.

5. Empirical momentum distribution

Here, we compare the calculated proton momentum distributions with experimental results extracted from the ${}^{12}\text{C}({}^3\text{He}, p)$ breakup cross-section measured at $p_{{}^3\text{He}} = 10.8 \text{ GeV}/c$ with the emission of the proton-fragments at 0° [4].

6

5.1. Empirical momentum distribution

To compare the calculated momentum distribution with experiment, it is necessary to establish a connection between the momentum \mathbf{K} (which is a theoretical quantity) and the measured proton momentum. In the non-relativistic case, it is of a common use to postulate that $\mathbf{K} = \mathbf{k}^*$, where \mathbf{k}^* is the proton momentum in the ${}^3\text{He}$ rest frame. But in the relativistic case, as that of the experiment [4], it is incorrect.

The more adequate description has been suggested long time ago within the so-called “minimal relativization scheme”. This approach was discussed in Ref. [19] in detail. Therefore, we recall only the main points here.

In the framework of this scheme, the momentum \mathbf{K} is to be identified with the “relativistic internal momentum” $\mathbf{k} = (\mathbf{k}_\perp, k_\parallel)$, which appears in the dynamics on the light front (LFD), instead of the non-relativistic \mathbf{k}^* . The LFD is often called as the “dynamics in the infinite momentum frame” (IMF). (The IMF is defined as a limiting reference frame, which is moving, with respect to the laboratory frame, in the negative z -direction with a velocity close to the speed of light.) In other words, it is the \mathbf{k} variable corresponding to the variable \mathbf{K} used in the previous sections. The important question is: “In which way the light-front variable \mathbf{k} is related to the measured momentum of a ${}^3\text{He}$ fragment?”

In the IMF dynamics, the wave function of a bound state is described in terms of two variables, α and \mathbf{k}_\perp . Let us consider ${}^3\text{He}$ as a (proton+ $2N$) system with masses m and \mathcal{M}_{2N} respectively; then α and \mathbf{k}_\perp are defined by

$$\alpha = \frac{E_p^{\text{lab}} + k_\parallel^{\text{lab}}}{E_{{}^3\text{He}}^{\text{lab}} + P_\parallel^{\text{lab}}}, \quad \mathbf{k}_\perp = \mathbf{k}_\perp^{\text{lab}}, \quad (15)$$

where $p = (E_p^{\text{lab}}, \mathbf{k}_\perp^{\text{lab}}, k_\parallel^{\text{lab}})$ and $P = (E_{{}^3\text{He}}^{\text{lab}}, \mathbf{0}_\perp, P_\parallel^{\text{lab}})$ are the proton and ${}^3\text{He}$ 4-momenta in the laboratory frame. In terms of α and \mathbf{k}_\perp , the effective mass squared of the $(p+2N)$ system becomes

$$\mathcal{M}_{p+2N}^2 = \frac{\alpha m^2 + (1 - \alpha) \mathcal{M}_{2N}^2 + \mathbf{k}_\perp^2}{\alpha(1 - \alpha)}, \quad (16)$$

and the longitudinal component of the \mathbf{k} momentum is given by

$$k_\parallel = \pm \sqrt{\frac{\lambda(\mathcal{M}_{p+2N}^2, \mathcal{M}_{2N}^2, m^2)}{4\mathcal{M}_{p+2N}^2} - \mathbf{k}_\perp^2}, \quad (17)$$

where $\lambda(a, b, c) = a^2 + b^2 + c^2 - 2ab - 2ac - 2bc$. In Ref. [19], it was argued that, because the mean momentum square in the pair $\langle q^2 \rangle \ll m^2$, one can take $\mathcal{M}_{2N} \approx 2m$.

From the kinematical conditions of experiment [4], it follows that $\mathbf{q}_\perp = 0$ and $\mathbf{k}_\perp = 0$. In this case, the signs "−" and "+" are chosen for $\alpha < \frac{1}{3}$ and $\alpha > \frac{1}{3}$, respectively; the IMF momentum \mathbf{k} is reduced to the momentum \mathbf{k}^* for $\alpha \approx \frac{1}{3}$.

The integral

$$\begin{aligned} & \int d^3k n_p(k) \\ &= \int_0^1 d\alpha \int d^2k_\perp \frac{\varepsilon_p(k)\varepsilon_{2N}(k)}{\alpha(1-\alpha)\mathcal{M}_{p+2N}^2} n_p(k) = 2, \quad (18) \\ \varepsilon_p(k) &= \sqrt{m^2 + k^2}, \quad \varepsilon_{2N}(k) = \sqrt{\mathcal{M}_{2N}^2 + k^2} \end{aligned}$$

gives the number of protons in ${}^3\text{He}$, and the following expression can be considered as the relativized momentum distribution of protons in ${}^3\text{He}$:

$$n_p^{\text{rel}}(\alpha, \mathbf{k}_\perp) = \frac{\varepsilon_p(k)\varepsilon_{2N}(k)}{\alpha(1-\alpha)\mathcal{M}_{p+2N}^2} n_p(k). \quad (19)$$

After that, in the framework of the IMF dynamics, the invariant differential cross-section of the $A({}^3\text{He}, p)$ breakup is given by

$$\begin{aligned} E_p \frac{d^3\sigma}{d\mathbf{p}_p} &= f_{\text{kin}}^{(p)} \sigma_d (1-\alpha) n_p^{\text{rel}}(\alpha, \mathbf{k}_\perp), \\ f_{\text{kin}}^{(p)} &= \frac{\lambda^{\frac{1}{2}}(W, \mathcal{M}_{2N}^2, M_A^2)}{2\alpha M_A P}, \end{aligned} \quad (20)$$

where W and M_A are the missing mass squared and the mass of the target nucleus, respectively; the σ_d factor plays the role of a normalization factors.

Equation (20) can be used to extract the proton momentum distribution in ${}^3\text{He}$.

It is clear that this equation was derived in the framework of the impulse approximation. Nevertheless, one may expect that the momentum distribution extracted from experimental data effectively includes effects beyond the impulse approximation, in particular, coming from the quark structure of ${}^3\text{He}$. Therefore it was called in Ref. [19] as "empirical momentum distributions" (EMD) of the protons in ${}^3\text{He}$.

5.2. Comparison with experiment

In Fig. 4, we compare results of our calculations for EMD extracted from data [4], as well as with the calculations of Ref. [19], based on 2N interactions only.

There is rather good agreement between calculations and EMD data at $k \lesssim 250$ MeV/c. At very small k ($\lesssim 50$ MeV/c) an enhancement of EMD data over theoretical curves is as obvious for the ${}^3\text{He}$ case as it was for the deuteron data. This effect may be naturally explained as a result of contributions of the Coulomb interaction to the breakup with the registration of a charged fragment at zero emission angle. Note that a similar enhancement takes place also in EMD of protons in a deuteron, extracted from data on the ${}^{12}\text{C}(d, p)$ breakup [22]. The results of calculations published in Ref. [23] and based on the Glauber-Sitenko model support the interpretation of this enhancement in the momentum distribution of protons in a deuteron as a manifestation of the Coulomb interaction. Of course, the final state interaction also might be significant in the region of small k . In case of the deuteron breakup, this effect was (in part, at least) taken into account in Ref. [23].

From the comparison of our results with EMD data under discussion, as well as with results published in Ref. [19] at $k > 250$ MeV/c, the following conclusions can be drawn:

- There is rather visible qualitative disagreement between the calculations and EMD of protons in ${}^3\text{He}$.
- Contribution of 3N interactions becomes significant in the $k > 250$ MeV/c region, but cannot explain completely the disagreement between the data on EMD of protons and calculations based on 2N interactions only.
- Version of the ${}^3\text{He}$ wave function based on the CDBN+TM potential looks more preferable than the version based on the AV18+U9 potential, because the latter strongly overestimates the existing EMD data at very high momenta (above 600 MeV/c).

6. Conclusions

The momentum distributions of neutrons and protons in ${}^3\text{He}$ have been calculated, by using the so-called "operator" form for the description of the 3N system.

We used results of Ref. [13], where the calculations of the necessary scalar functions (appearing in the operator form representation of the bound 3N system) were performed with two potentials, which involve the effective 3N interactions, 2N interaction AV18 [14] with the interaction Urbana-IX [15] (AV18+U9), and 2N interaction CD-Bonn [16] with insertion of the 3N Tucson-Melbourne interaction [17] (CDBN+TM).

We compare our results with calculations of Ref. [19], which do not take the 3N interactions into account, and conclude that the 3N interactions become essential at the large internal momentum $K > 250$ MeV/ c of a nucleon in the bound 3N system.

We also compare the calculated momentum distribution of protons with the so-called empirical momentum distribution in ${}^3\text{He}$, extracted from the $({}^3\text{He}, p)$ breakup cross-section [22], and conclude that 3N interactions reduce the disagreement between theory and experiment at $k > 250$ MeV/ c . Nevertheless, this disagreement does not completely disappear even in the case where the 3N interactions are taken into account.

That means, that non-nucleonic degrees of freedom in ${}^3\text{He}$, as well as mechanisms beyond the so-called “impulse approximation” become important in the ${}^3\text{He}$ breakup at $k > 250$ MeV/ c and all other processes, where the nucleon-constituents of this nucleus (as well as other nuclei) are very close (at distances < 0.8 fm) to each other.

1. K. Ermisch et al., Phys. Rev. C **71**, 064004 (2005).
2. H. Kamada, O. Shebeko, and A. Arslanaliev, Few-Body Syst. **58**, 70 (2017).
3. I. Dubovyk and O. Shebeko, Few Body Syst. **48**, 109 (2010).
4. V.G. Ableev et al., JETP Lett. **45**, 596 (1987); Pis'ma v ZhETP **45**, 467 (1987).
5. V. Baru, J. Haidenbauer, C. Hanhart, J.A. Niskanen, Eur. Phys. J. **A 16**, 437 (2003).
6. V.V. Kotlyar and A.V. Shebeko, Zeitschrift für Physik A **327**, 301 (1987).
7. V.V. Kotlyar and A.A. Shcheglova, Vist. Khark. Univ. N° 832, Ser. Fiz. “Yad., Chast., Polya”, Issue 4 (40), 11 (2008).
8. V. Kotlyar and J. Jourdan, Problems of Atomic Science and Technology. Series: Nucl. Phys. Investigations **6(45)**, 24 (2005).
9. E. Gerjuoy and J. Schwinger, Phys. Rev. **61**, 138 (1942).
10. W. Rarita and J. Schwinger, Phys. Rev. **59**, 436 (1941); Phys. Rev. **59**, 556 (1941).
11. I.V. Simenog, I.S. Dotsenko, and B.E. Grinyuk, Ukr. J. Phys. **47**, 129 (2002).
12. I.S. Dotsenko and I.V. Simenog, Ukr. J. Phys. **51**, 841 (2006).
13. I. Fachruddin, W. Glöckle, Ch. Elster, and A. Nogga, Phys. Rev. C **69**, 064002 (2004).
14. R.B. Wiringa, V.G.J. Stoks, and R. Schiavilla, Phys. Rev. C **51**, 38 (1995).
15. B.S. Pudliner et al., Phys. Rev. C **56**, 1720 (1997).
16. R. Machleidt, Phys. Rev. C **63**, 024001 (2001).
17. S.A. Coon et al., Nucl. Phys. A **317**, 242 (1979); S.A. Coon and W. Glöckle, Phys. Rev. C **23**, 1790 (1981).
18. <http://www.phy.ohiou.edu/~elster/h3wave>
19. A.P. Kobushkin and E.A. Strokovsky, Phys. Rev. C **87**, 024002 (2013).
20. R. Schiavilla, V.R. Pandharipande, and R.B. Wiringa, Nucl. Phys. A **449**, 219 (1986).
21. M. Lacombe et al., Phys. Rev. C **21**, 861 (1980).
22. V.G. Ableev et al., Nucl. Phys. A **393**, 491 (1983) and A **411**, 541 (E) (1983); V.G. Ableev et al., JINR Rapid Comm. 1[52]-92 10 (1992); V.G. Ableev et al., JINR Rapid Comm. 1[52]-92 5 (1992) and Yad. Fiz. **37**, 132 (1983).
23. A.P. Kobushkin and Ya.D. Krivenko-Emetov, Ukr. J. Phys. **53**, 751 (2008).